JOURNAL OF MATERIALS SCIENCE 16 (1981) 2119–2129

# A method for evaluating the thermal fatigue resistance of ceramics and its application to a fibre reinforced refractory material

J. LAMON
*Centres des Matériaux de l'Ecole des Mines de Paris, BP 87, 91003 Evry Cedex, France*

An original method of characterizing thermal fatigue of ceramic materials has been proposed. This method is based on after-shock measurements of the degree of damage through a compliance calibration using compact tension (CT) test pieces. This method has been applied to a fibre-reinforced refractory material subjected to repeated thermal shock between 20 and 800° C. It has been demonstrated from both experiments and finite element analysis that the CT specimen is a convenient shape for the evaluation of thermal fatigue behaviour. In these specimens it has been established that the damage primarily affects the notch tip. The thermal fatigue behaviour of the CT specimens depends on notch length: when the notch length is greater than 30 mm, catastrophic failure occurs after a few cycles. When the notch length is less than 30 mm, the crack formed at the notch tip during the first cycle grows slowly during subsequent cycles. This behaviour has been explained by the variation of the stress intensity factor $K_I$.

## 1. Introduction

Thermal fatigue is one of the primary origins of failure in ceramic materials used in practical applications. So far only a few studies have dealt with the behaviour of ceramics under repeated thermal shock. Most of the methods involve characterizing the resistance of ceramics to a single cooling. They are based on simplifying assumptions dealing with microstructure and fracture; for example, flaws are neglected [1] or assumed to be circular and distributed uniformly throughout the material [2] and crack initiation is supposed to occur at surface-located flaws [1, 3]. The methods proposed to predict thermal fatigue consist generally of a numerical [4] or analytical [5] simulation of crack propagation using tedious and complex calculations. Moreover, a large variety of thermal stress tests have been employed. For example, one test consists of measuring thermal shock resistance as a function of the decrease in elastic properties [6] or strength [2]; a second type consists of simulated service tests such as the ASTM panel spalling tests [7]. In the typical case of thermal fatigue a type of test generally used consists of measuring the thermal fatigue resistance by the number of cycles required to result in complete failure [8–10]. However, it seems that it is impossible to measure the extent of crack propagation in a single sample due to thermal fatigue with the help of the methods proposed [1, 5, 8, 9].

In the present paper, an original method will be presented of following the evolution of the damage produced under thermal shock conditions in a single sample of ceramic material. This method is based on after-shock measurements of the degree of damage through a compliance calibration. Notched compact tension (CT) test pieces have been used, which because of their shape, offer the important advantage that the thermal shock fracture occurs at the notch tip. This result was obtained by a thermal stress analysis using the numerical finite element method and was then confirmed by experiment.

In the work reported here, this method has been employed to study the behaviour of a fibre-reinforced refractory material subjected to thermal shock between 20 and 800° C. This material constitutes the structure of an industrial electromagnetic pump for liquid aluminium.

0022–2461/81/082119–11$03.10/0  

## 2. Experimental procedure

### 2.1. Specimens

The specimens were made of an industrial composite refractory material, consisting of short mullite fibres (size $< 1$ mm) in a matrix of alumina-based cement (Secar*). The chemical composition is given in Table I. Fibres were randomly distributed throughout the material. The fraction of fibres was 60 wt%. Most pores included in the matrix were very small (smaller than 20 $\mu$m for 95 vol%). Some larger pores were also present with diameters up to 1 mm.

Because of this microstructure, this material exhibits a specific mechanical behaviour [11] which determines its thermal fatigue behaviour. The failure process can be divided into two stages [11]. During the first stage, microcracking took place, followed by macrocracking. Typically microcracks begin to form at low loads in the vicinity of the notch tip, generating a damaged zone which behaves inelastically in a way, analogous to the crack-tip plastic zone in metals [11, 12]. During the second stage, crack growth took place and fibres are pulled out from the matrix. Crack growth is accompanied by microcracking ahead of the crack tip, similar to that observed prior to initial macroscopic cracking. In addition, at the temperatures we were interested in (800° C) no effect of temperature on the material structure was observed in air [11]. However, when held for long time at higher temperatures (above 1000° C), the material showed a decrease in the specific surface area of open porosity. Finally, the mechanical properties were not significantly affected by thermal conditions in air up to 800° C. Thus, for example, measurements of fracture energy at 800° C gave values similar to those obtained at room temperature, suggesting that there were no strong environmental effects on crack propagation at this temperature. Therefore, it can be assumed that under thermal shock between room temperature and 800° C, crack growth was primarily caused by thermal stresses.

### 2.2. Experimental procedure and apparatus

The CT test pieces were designed according to ASTM standard recommendations for steels [13]. The dimensions are shown in Fig. 1, and the recommended relationships between the dimensions are included. A tensile testing machine (Instron) with a constant cross-head velocity of 0.2 mm min$^{-1}$ was used to measure the residual compliance. During the test, crack opening displacement was measured by means of a "clip gauge" attached to the specimens as shown schematically in Fig. 2. The gauge was composed of two cantilever beams separated by a spacer-block. Load was measured by a conventional load-cell (Instron). Load and displacement were plotted on an $X-Y$ recorder. The compliance was measured without exceeding the linear elastic regime. Typical load–displacement curves are shown in Fig. 3. The compliance is the recipocal of the slope of this curve. For each specimen, four curves were plotted (Fig. 3) and the compliance was calculated as the median value of the slope.

Specimens were subjected to repeated cycles of heating and rapid cooling and their compliance was evaluated after a varying number of thermal cycles: after each cycle for the first five cycles, then after 5 cycles, after 10 cycles etc. Heating was performed in an electric furnace for about 1.5 h until equilibrium was attained. The temperature of the hot zone in the furnace was equal to 800 ± 6° C. Specimens were cooled by a current of compressed air at about 20° C. They were held

TABLE I Properties of material

| | | |
|---|---|---|
| *Chemical analysis* | | |
| $Al_2O_3$ | fibres: | 51% |
| | matrix: | 33% |
| CaO | matrix: | 7% |
| $SiO_2$ | fibres: | 9% |
| *Physical properties* | | |
| Density ($d$): | | 1.2 |
| Open porosity: | | 50% (pore diameter $< 25$ $\mu$m) |
| Closed porosity: | | 10% |
| BET specific surface area: | | $30 \times 10^3$ m$^2$ kg$^{-1}$ |
| *Thermal properties* | | |
| Specific heat ($C_p$): | | $1.254 \times 10^3$ J kg$^{-1}$ ° C$^{-1}$ |
| Thermal conductivity ($K$): | | 0.3 W m$^{-1}$ ° C$^{-1}$ at 300° C |
| | | 0.4 W m$^{-1}$ ° C$^{-1}$ at 1000° C |
| Thermal diffusivity: | | $2.5 \times 10^{-7}$ m$^2$ sec$^{-1}$ |
| Linear thermal expansion coefficient ($\alpha$): | | $5 \times 10^{-6}$ ° C$^{-1}$ |
| *Mechanical properties* | | |
| Young's modulus ($E$): | | 2000 MN m$^{-2}$ |
| Compressive strength: | | 15 MN m$^{-2}$ |
| Tensile strength: | | 1.4 MN m$^{-2}$ |
| Flexural strength (3 points): | | 2.3 MN m$^{-2}$ |
| Fracture energy ($\gamma$): | | 60 J m$^{-2}$ |
| Poisson's ratio ($\nu$): | | 0.25 |

*Obtained from Novatome Co., Montlhéry, France.

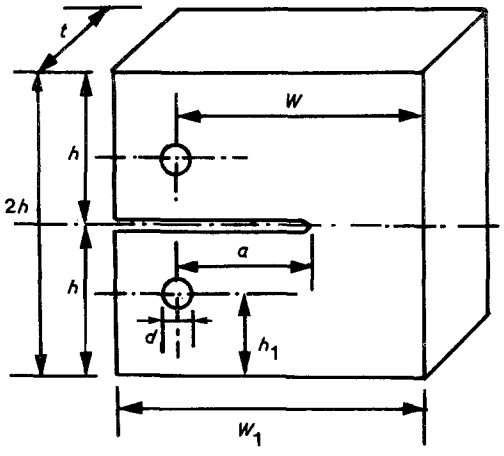


$W = 2t = 40\,mm$

$h = 1.2t = 24\,mm$

$d = 5\,mm$

$W_1 = 2.5t = 50\,mm$

$h_1 = 0.65t \approx 13\,mm$

$t = 20\,mm$

*Figure 1* Dimensions of the compact tension specimens and the relationships between the dimensions recommended by the ASTM.

in compressed air for 30 min. Six specimens were charged in the specimen holder as shown in Fig. 4, so that heat transfer occurred exclusively through the lateral surfaces of specimens. The time for transfer from the furnace into the current of compressed air was about 0.8 sec. Transfer from the current of compressed air into the furnace took about 2 sec.

## 3. Material damage measurement

The damage caused by thermal cycling was characterized by after-shock compliance measurements using the specific compliance calibration curve $C = f(a)$; to be valid such a method requires that the damage occurs at the notch tip of the CT specimens. To check the validity of such a method, firstly, the distribution of thermal stresses in rapidly-cooled specimens was calculated using the numerical finite element method and, secondly, an experimental determination was made of the contribution of the different parts of shocked specimens to the compliance change.

### 3.1. Specific compliance calibration curve $C = f(a)$

The specific compliance calibration curve $C = f(a)$ was determined by both an experimental method and an analytical method. The experimental method consisted of determining the compliance of unshocked specimens with varying notch lengths. The analytical method was based on the stress intensity factor $K_I$ and the rate of energy release $G_I$. This method uses the known relationships between compliance and $G_I$, between $G_I$ and $K_I$ and between $K_I$ and the crack length $a$ (see Appendix).

The agreement between the experimental compliance calibration curve $C = f(a)$ and the theoretical curve is excellent (Fig. 5). This result establishes that linear fracture mechanics concepts can be applied to this material with a good degree of accuracy despite microscopic heterogeneity. In addition, the large notch radius ($> 0.5$ mm, the size of the more serious pre-existing flaws in the material) has no significant effect on compliance measurements (Fig. 6).

Using the compliance calibration curve $C = f(a)$, the damage can be characterized for any shocked specimen, providing the damage consists of a macrocrack. In the typical case of microcracks, the extent of the microcracked region will be

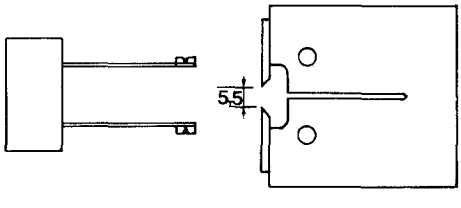


*Figure 2* Clip gauge and method of mounting on CT specimens for crack-opening displacement measurement.

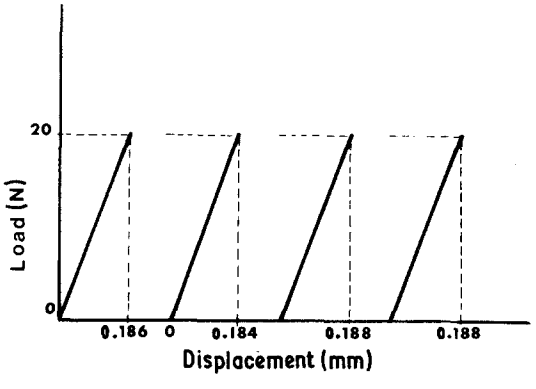


*Figure 3* Load–displacement curves (linear elastic regime).

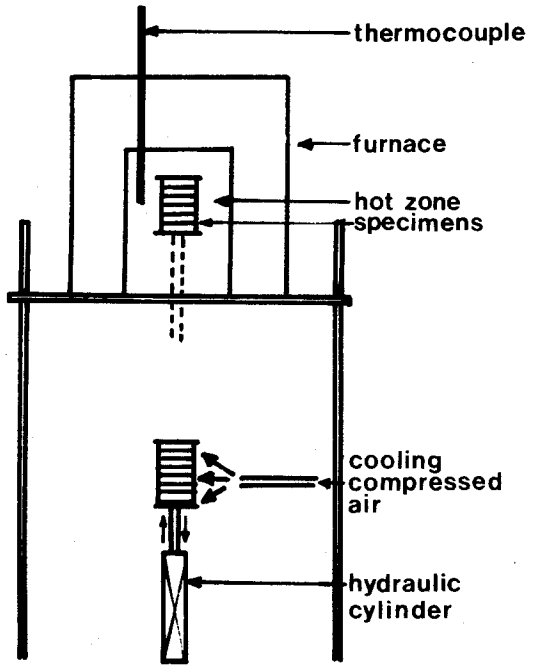


*Figure 4* Schematic diagram of the thermal fatigue testing apparatus.

characterized by an equivalent crack such that its size corresponds to the compliance of the specimen.

## 3.2. Validity of the compliance technique

Thermal stresses have been calculated in the typical case of an undamaged CT specimen subjected to a single severe cooling. A conventional two-dimensional elastic finite element technique was

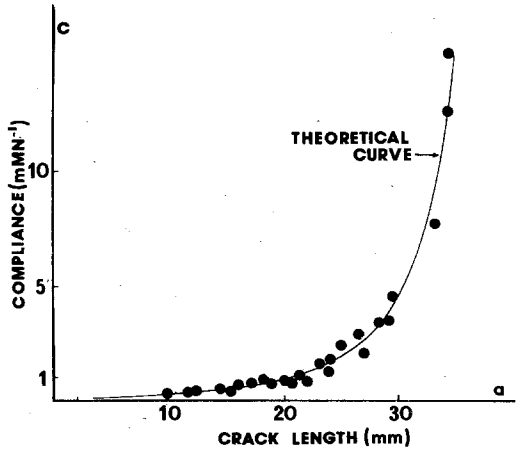


*Figure 5* Experimental and theoretical compliance calibration curves $C = f(a)$.

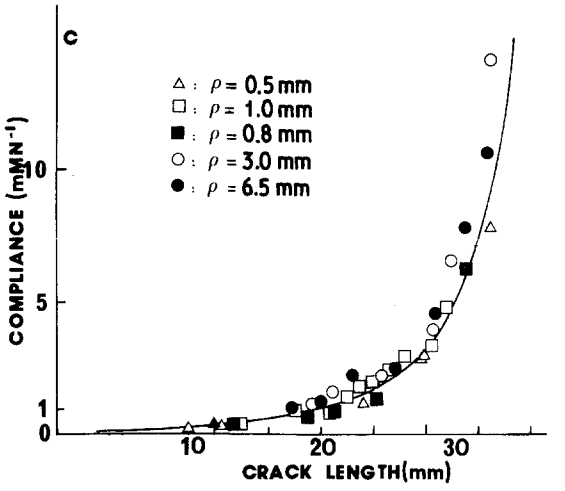


*Figure 6* Effect of notch radius, $\rho$, on compliance calibration curve $C = f(a)$.

employed. A computer program was used to determine transient temperature distributions and a second, compatible program was used to determine the elastic stress and strain fields (the SAP4 finite element program*). Three different notch configurations were considered: first, the surface of the notch was supposed to be insulated (notch length = 20 mm), and second and third, the surface of the notch was insulated, but notch lengths were 20 and 32 mm, respectively. The corresponding finite element meshes are shown in Figs 7 to 9.

It was assumed that the specimen had a uniform initial temperature equal to 800° C ($t = 0$), and that the surface was maintained at a constant temperature of 20° C from the time $t = 0.01$ sec (except for the insulated surface notch). Such conditions are much more severe than the conditions the specimens were subjected to during thermal fatigue experiments. Thus, the heat transfer coefficient corresponding to the boundary conditions of thermal analysis was infinite; while the value corresponding to experiment conditions was about 40 $W m^{-2} ° C^{-1} sec^{-1}$. Consequently, it is clear that the thermal stresses were overestimated. There is no reason why their distributions should be different.

The material was assumed to be homogeneous, elastic and isotropic. Only stresses arising from temperature gradients have been taken into account and microstresses and stresses arising from the difference in expansion between phases have not been considered.

*Developed by Novatome Co., Le Plessis Robinson, France, 1977.

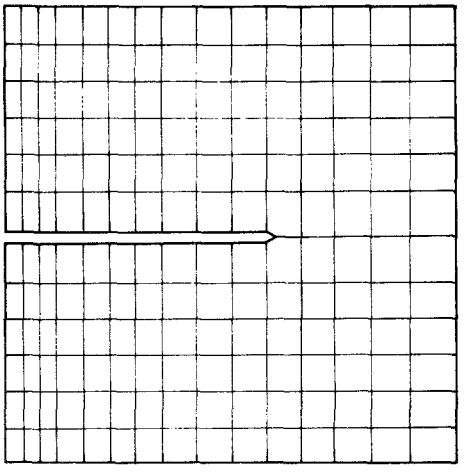

*Figure 7* Finite element mesh for the case of an insulated surface notch (notch length = 20 mm).

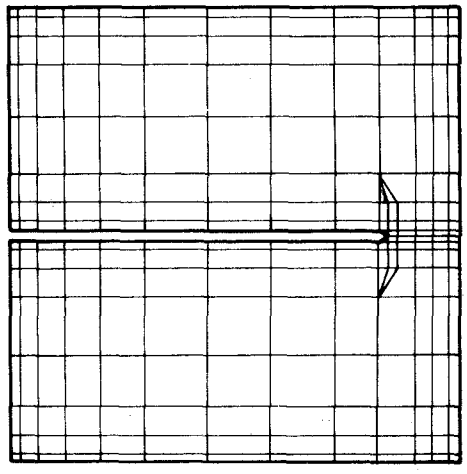

*Figure 9* Finite element mesh for the case of an uninsulated notch (notch length = 32 mm).

### 3.2.1. Thermal stress analysis

For the case of an uninsulated notch (Fig. 10) during the shock of cooling, the stress field in CT specimens may be divided into three distinct zones:

Zone 1 in which the surface is in tension and the dominant component of the tensile stress is parallel to the surface.

Zone 2 in which the centre is in compression.

Zone 3 in which in the vicinity of notch tip there is a compression–tension stress field.

At the notch tip, the dominant tensile stresses act in a direction normal to the notch plane (Mode I notch opening). The maximum tensile stress is greater at the notch tip than in any other part of specimen, especially if the notch length is small. For example the maximum tensile stress in this region is about 17 MN m$^{-2}$ when the notch length is 20 mm, and about 10 MN m$^{-2}$ when the notch length is 32 mm, while the tensile stress is less than 10 MN m$^{-2}$ in the rest of Zone 1 (see Fig. 10), and less than 1 MN m$^{-2}$ in Zone 3. It is clear that under stress conditions, damage will primarily occur at the notch tip even though additional damage may occur in Zones 1 and 3 because of the tensile stresses in these regions.

In the centre of the specimens, the maximum compressive stress (5 MN m$^{-2}$) is less than the

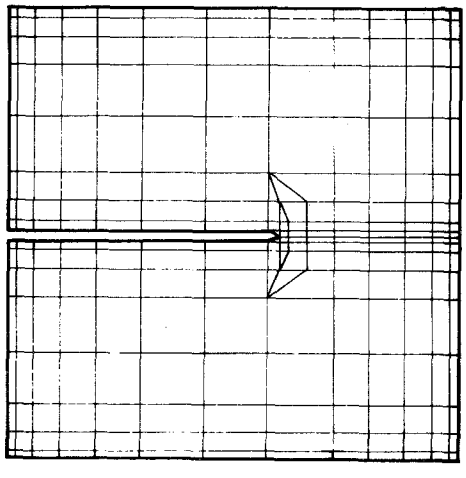

*Figure 8* Finite element mesh for the case of an uninsulated notch (notch length = 20 mm).

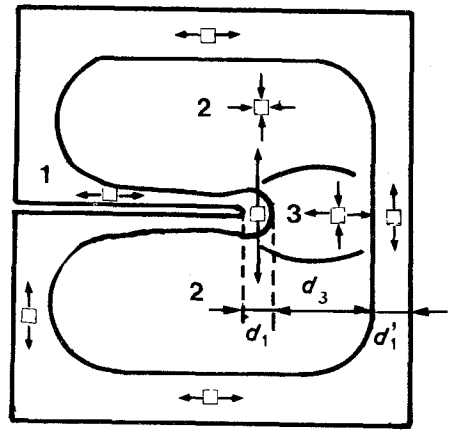


| $a_0$ | $d_1$ | $d_3$ | $d_1'$ |
|---|---|---|---|
| 20mm | 3mm | 13mm | 4mm |
| 32mm | 1mm | 4mm | 3mm |

*Figure 10* Thermal stress field for a single cooling shock in the case of a CT specimen having an uninsulated notch.

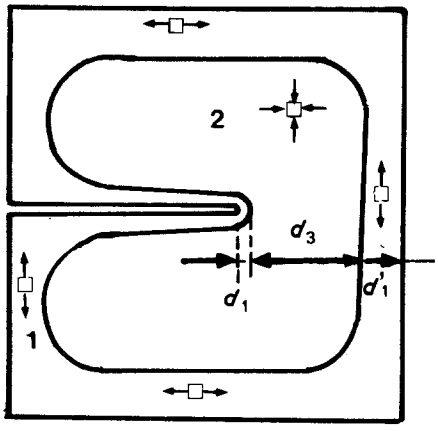


| $d_1$ | $d_3$ | $d'_1$ |
|---|---|---|
| 2mm | 14mm | 4mm |

*Figure 11* Thermal stress field for a single cooling shock in the case of a CT specimen having an insulated surface notch.

compressive strength ($15\,MN\,m^{-2}$) so that no damage should occur.

If the notch surfaces are insulated, the stress field may be divided into only two distinct zones: the surface (Zone 1) and the centre (Zone 2) which are in tension and compression respectively (Fig. 11), The tensile stresses at the surface of the notch are negligible. The maximum stress is less than $10^{-2}\,MN\,m^{-2}$. However, the maximum tensile stress at the external surface is the same as that obtained previously for specimens with non-insulated notch surfaces ($10\,MN\,m^{-2}$). This result indicates that damage may occur at the surface exclusively and will be comparable in extent to that detected in specimens with non-insulated notches. These results are of paramount importance in evaluating the effect of surface damage on compliance changes.

### *3.2.2. Location of damage in CT specimens*

The increase in compliance caused by the thermal shock of cooling may be regarded as the sum of the two compliance changes $\Delta C_E$ and $\Delta C_S$ caused by notch tip damage and surface damage respectively. In addition, it is well known that on heating the inverse stress field is obtained, so that Zones 2 and 3 which were in compression on cooling, will be in tension on heating. This suggests that on heating, CT specimens may be affected by further damage which could cause an additional increase in compliance $\Delta C_c$. Thus, the total increase in compliance after one cycle of heating and cooling, $\Delta C$, may be regarded as the sum of the different compliance changes $\Delta C_c$, $\Delta C_E$ and $\Delta C_S$

$$\Delta C = \Delta C_c + \Delta C_S + \Delta C_E. \qquad (1)$$

To estimate the magnitude of the compliance change $\Delta C_c$ resulting from heating, CT specimens have been subjected to thermal cycles under cooling conditions such that no damage may occur on cooling (slow cooling over about 3.5 h). From these experiments it appears that compliance changes $\Delta C_E$ are negligible (Fig. 12). This establishes that heating shocks have no significant effect on total compliance changes $\Delta C$.

To estimate the magnitude of $\Delta C_S$, CT specimens having insulated notches were subjected to repeated thermal cycles of heating and cooling. Notches were insulated with pyronap attached to the surface. Thermal conditions have been described previously (see Section 2.2). Fig. 12 shows that compliance changes are not significant compared with changes observed for specimens having an uninsulated notch. This result establishes that the influence of surface damage on compliance changes may be considered as negligible.

In summary, the increase in compliance observed after repeated cycles of heating and cooling may be attributed to the damage created on cooling at the notch tip exclusively.

## 4. Results

Fig. 13 shows that the thermal fatigue behaviour of CT specimens depends on notch length. For a notch length greater than 30 mm (long notches) catastrophic failure occurs after a few cycles and a crack can be detected at the notch tip by direct observation after the first cycles. For notch lengths less than 30 mm (short notches), the growth of the damage exhibits three distinct stages: in the first stage which generally corresponds to the first cycle, the damage is greatest; in the second stage the damage growth per cycle decreases and, in the third stage it is slow. For short notch specimens macroscopic cracks were rarely directly observed: only after about 300 cycles for two specimens and after about 25 cycles for a third specimen. In contrast to the long notch specimens no damage was observed for the first cycles. Nevertheless, several results suggest that the damage in the first cycle is a single crack rather than microcracks:

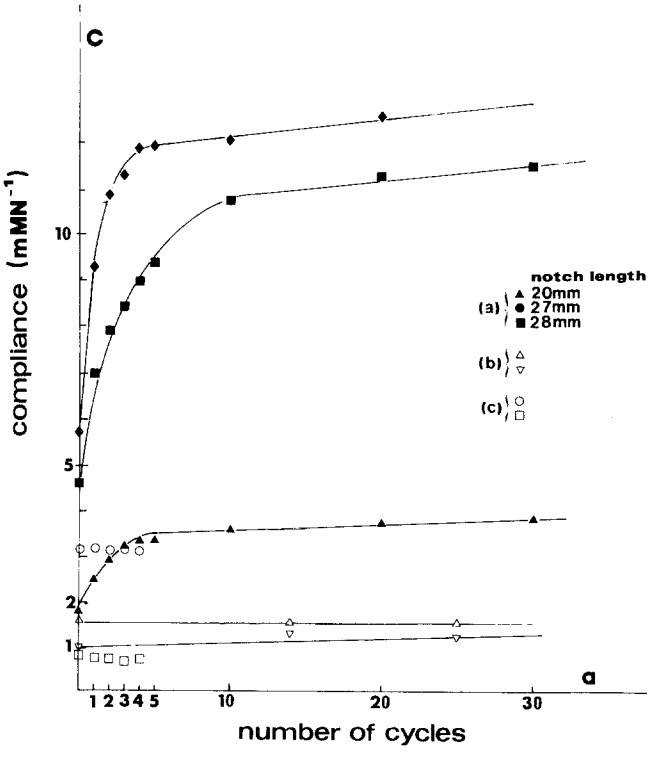


*Figure 12* Variation of compliance with the number of cycles under varying conditions: (a) thermal cycles as defined in Section 2.2 in the case of an uninsulated notch, (b) thermal cycles as defined in Section 2.2 in the case of an insulated notch and (c) thermal cycles with slow cooling (3.5 h).

Firstly, the equivalent crack length is similar to the size of the crack observed previously with the long notched specimens, that is, about 2 mm in all cases (see Table II).

Secondly, as demonstrated by thermal analysis, tensile stresses at the notch tip are greater in short notched specimens than in long notched specimens.

It is concluded that conditions for fracture in the first cycle are more favourable for short notched specimens than for long notched specimens. In subsequent cycles, the rate of damage decreases rapidly. As reported in Table III, the median value for the growth rate of the equivalent crack is less than 1 mm per cycle in the second cycle, and less than 0.1 mm per cycle for the tenth cycle. This suggests that the crack created during

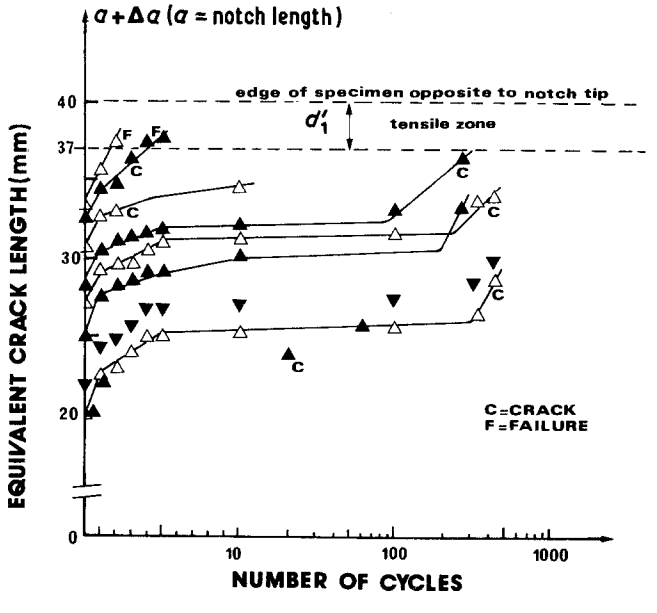


*Figure 13* Variation of the equivalent crack length, $\Delta a$, with the number of cycles.

TABLE II Variation of $\Delta a$, the equivalent crack length with the number of cycles

| Notch length (mm) | Number of cycles | | | | | | | | | | | | | |
|---|---|---|---|---|---|---|---|---|---|---|---|---|---|---|
| | 1 | 2 | 3 | 4 | 5 | 10 | 20 | 40 | 60 | 100 | 120 | 283 | 340 | 472 |
| 20 | 2.2 | | | | | | 3.8 | | 5.8 | | | | | |
| 21.8 | 2.5 | 3 | 4 | 5 | 5 | 5.2 | | | | 5.6 | | | 6.6 | 8 |
| 24.7 | 2.2 | 3.2 | 3.6 | | | 5 | 5.2 | 6.2 | | | 7.6 | 8.2 | | |
| 27.5 | 2.1 | 2.6 | 2.8 | 3.4 | 4 | 4.2 | | | | 4.5 | | | 6.6 | 6.8 |
| 27.9 | | | | | | 3.1 | 4.2 | 5.9 | 6.3 | | 7.9 | 8.2 | | |
| 28.3 | 2.3 | 3 | 3.2 | 3.4 | 3.5 | 3.6 | | | | 4.0 | | | | |
| 30.4 | 2.2 | 2.6 | | | | 4.2 | | | | | | | | |
| 31.2 | 4.0 | 4.4 | | | | | | | | | | | | |
| 32.3 | 1.8 | 2.3 | | 3.8 | 4.8 | 5 | | | | | | | | |
| 33.1 | 2.2 | 4.2 | | | | | | | | | | | | |

the first cycle propagates by the formation of microcracks during subsequent cycles. In short notched specimens the rate of slow damage growth does not depend on notch length. In Table III it can be seen that damage growth rate is not enhanced by an increase in notch length. Consequently, the differences in the damage growth rate observed with different specimens cannot be attributed to an effect of notch length but is rather due to the pre-existing flaws whose distribution varies from specimen to specimen.

## 5. Discussion

The behaviour of a crack in a thermal stress field is determined by the variations of the stress intensity factor $K_I$ [14]. The determination of the relationship between $K_I$ and crack length, $a$, is a complex problem which, in general, can be solved using numerical techniques only for given specimen geometries. An analytical solution is available only for a particular configuration of short cracks [14]. For large cracks, the $K_I$–crack length relationship can only be obtained numerically. However, for CT specimens qualitative variations of $K_I$ with thermal cycling can be determined using some features of thermal stress given in the literature [15, 16] together with thermal stress analysis (see Section 3.2). These properties deal with the variation and magnitude of thermal stress. The variation of tensile thermal stress with time of cooling is well known [1, 17, 18]. As shown schematically in Fig. 14, thermal stress exhibits a maximum at a time depending on the boundary conditions while the magnitude of this maximum decreases as the distance from the surface increases, corresponding to the decreasing temperature gradient. There is no reason why these results should not be applied to the CT specimen stress field.

The crack length is similar to the width of the zone placed in tension during the first cycle (about 3 mm, see Table II and Fig. 10), and is generally larger than this zone during the following cycles (see Table II). As established by several authors [14, 19, 20], a crack modifies the local stress distribution as it propagates. It will now be demonstrated that the crack is subjected to tensile stresses during each cycle, owing to the specific origin of the thermal stress (which is generated by the difference in thermal expansion of various parts of the body [1, 17]). As noted previously, the effect of thermal shock during

TABLE III Variation of $\Delta a/\Delta N$, the growth rate of the equivalent crack (per cycle) with the number of cycles

| Notch length (mm) | Number of cycles | | | | | | | | | | | | | |
|---|---|---|---|---|---|---|---|---|---|---|---|---|---|---|
| | 1 | 2 | 3 | 4 | 5 | 10 | 20 | 40 | 60 | 100 | 120 | 283 | 340 | 472 |
| | Stage I | Stage II | | | | | Stage III | | | | | | | |
| 20 | 2.2 | | | | | | 0.067 | | 0.09 | | | | | |
| 21.8 | 2.5 | 0.5 | 1 | 1 | 0 | 0.4 | | | | 0.004 | | | 0.004 | 0.01 |
| 24.7 | 2.2 | 1 | 0.4 | | | 0.16 | 0.015 | 0.067 | | | 0.018 | 0.004 | | |
| 27.5 | 2.1 | 0.5 | 0.2 | 0.6 | 0.6 | 0.04 | | | | 0.003 | | | 0.009 | 0.004 |
| 27.9 | | | | | | | 0.085 | 0.11 | 0.01 | | 0.034 | 0.004 | | |
| 28.3 | 2.3 | 0.7 | 0.2 | 0.2 | 0.1 | 0.02 | | | | 0.004 | | | | |
| 30.4 | 2.2 | 0.4 | | | | 0.2 | | | | | | | | |

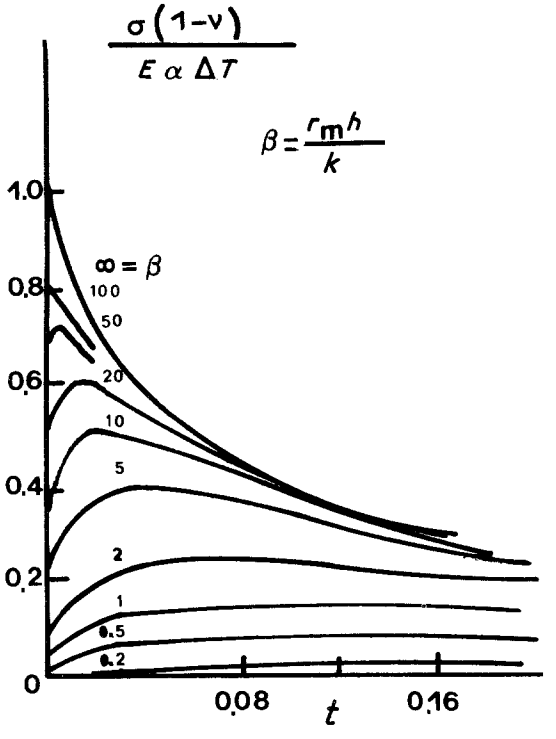


*Figure 14* Dimensionless stress against dimensionless time for various values of dimensionless heat transfer [18].

heating is negligible so that only the thermal shock due to cooling will be considered. Points on the surface of the crack are free to move normal to the crack plane, so that, on cooling, they cannot prevent contraction in this direction; nor can the crack surface affect the compatibility of the volume elements. Consequently, the tensile zone existing at the notch tip before the crack was created will be extended so that the whole crack will now be included in this tenzile zone.

For each cycle, the variation of $K_I$ with time is similar to the variation of the tensile thermal stress (Fig. 15), as indicated by the relationship between $K_I$ and thermal stress

$$K_I = \sigma Y a^{\frac{1}{2}}, \tag{2}$$

where $Y$ is a geometrical factor, $\sigma$ is the tensile thermal stress acting on the crack and $a$ is the crack length. But, when $K_I$ is equal to the maximum $K_{I,max}$, thermal stress decreases as demonstrated from the condition $dK_I/dt = 0$ where

$$\sigma_m = -\frac{2\dot{\sigma}_m a_m}{\dot{a}_m}, \tag{3}$$

where $\sigma_m$ is the stress corresponding to $K_{I,max}$, $a_m$ and $\dot{a}_m$ are the values of $a$ and $\dot{a}$ $(= da/dt)$ corresponding to $K_{I,max}$ and $\sigma_m$ is the value of $\dot{\sigma}$ $(= d\sigma/dt)$ corresponding to $K_{I,max}$. It appears that the slope $\dot{\sigma}_m$ must be $\langle 0$ so that $\sigma_m \rangle 0$.

The conditions for the onset of microcracking and macrocracking (see Section 2.1) are bounded by the critical values of the stress intensity factor $K_0$, $K_I^*$ and $K_{IC}$, where $K_0$ corresponds to the elastic limit of the material ($K_0 = 0.14\,MN\,m^{-3/2}$) and indicates the beginning of microcracking, $K_I^*$ indicates the onset of macrocracking ($K_I^* = 0.3\,MN\,m^{-3/2}$) while $K_{IC}$ corresponds to complete failure ($K_{IC} = 0.5\,MN\,m^{-3/2}$). Crack growth in CT specimens subjected to thermal fatigue can be described by the variation of the maximum value of the stress intensity factor, $K_{I,max}$, with the number of cycles. Damage occurs if $K_I$ is greater than $K_0$ and is dependent on the magnitude of $K_{I,max}$ compared with $K_I^*$. For short notched specimens the three stages observed in fracture can be attributed to a decrease in $K_{I,max}$ caused by a decrease in the temperature gradient at the crack tip as the crack propagates. Thus, because of the decrease in temperature gradient, the tensile thermal stress decreases with the number of cycles and, consequently, the magnitude of $K_{I,max}$ decreases also. It may be concluded that $K_{I,max}$ is greater than $K_I^*$ during the first cycles and is less than $K_I^*$ during the microcracking stage.

For the long notched specimens as shown in Fig. 13, the crack reaches the tensile zone opposite the notch tip only after a few cycles. Consequently the magnitude of the stresses acting on the crack tip is great and microcracking is less important. Long notched specimens have limited applications, because crack growth is too rapid to judge the thermal fatigue behaviour. Moreover, the extent of the damage cannot be deduced

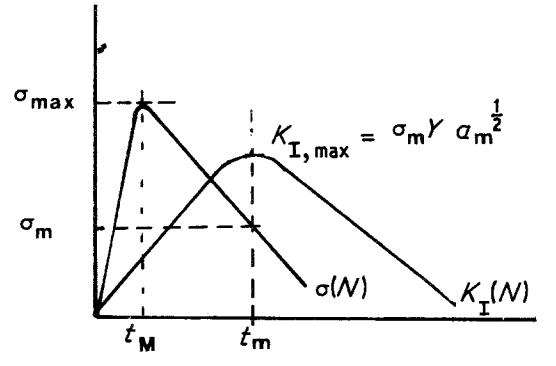


*Figure 15* Thermal stress and stress intensity factor at the crack tip against time of cooling.

sufficiently accurately from the compliance calibration curve $C = f(a)$.

## 6. Conclusion

It has been demonstrated that compliance measurements can be used to evaluate the effect of thermal fatigue on the refractory composite material studied here. Both experiments and finite element analysis have shown that the CT specimen is a convenient shape for the evaluation of thermal fatigue behaviour. As a result it has been established that the damage primarily affects the notch tip and that observed compliance changes are caused exclusively by the damage created at the notch tip. The extent of damage was deduced from the compliance calibration curve $C = f(a)$. It was found that the notch length must not exceed 30 mm. When the notch length was less than 30 mm, a crack formed at the notch tip in the first cycle which grew microscopically during the following cycles. This particular mode of slow crack growth seems to be due to the specific properties of this material, and particularly the inelastic behaviour induced by microcracking before crack formation.


## Acknowledgements

The author is grateful to Professor Mocellin (Ecole Polytechnique de Lausanne) for his assistance in certain phases of this work.


## Appendix: Analytical determination of the compliance relation $C = f(a)$

For plane strain conditions, the strain energy release rate $G_I$ is related to the compliance and to the stress intensity factor $K_I$ by the relationships

$$G_I = \frac{P^2}{2t} \cdot \frac{\partial C}{\partial a} \tag{A1}$$

and

$$G_I = \frac{K_I^2}{E}(1-\nu^2), \tag{A2}$$

where $P$ is the load, $E$ is Young's modulus and $\nu$ is Poisson's ratio. Substituting Equation A2 into Equation A1

$$dC = 2t\,\frac{1-\nu^2}{E}\,\frac{K_I^2}{P^2}\,da. \tag{A3}$$

The stress intensity factor $K_I$ is generally expressed in the following form

$$K_I = \frac{PY}{tW^{\frac{1}{2}}}, \tag{A4}$$

where the function $Y = f(a/W)$ accounts for configuration, and $W$ is the specimen width (see Fig. 1).

The function $Y$ has been determined for many types of loading and configurations [21]. For the compact tension specimen configuration, the $Y$ function is

$$Y = \left(\frac{a}{W}\right)^{\frac{1}{2}}\left[29.6 - 185.5\,\frac{a}{W} + 655.7\left(\frac{a}{W}\right)^2 - 1017\left(\frac{a}{W}\right)^3 + 638.9\left(\frac{a}{W}\right)^4\right]. \tag{A5}$$

Substituting Equation A4 into Equation A3

$$dC = \frac{1-\nu^2}{E} \cdot \frac{2Y^2}{tW}\,da. \tag{A6}$$

The function $Y$ may be expressed as

$$Y = \left(\frac{a}{W}\right)^{\frac{1}{2}} \sum_{i=1}^{5} \theta_i \left(\frac{a}{W}\right)^{i-1}, \tag{A7}$$

where $\theta_i$ is a series of coefficients. Thus for $Y^2$

$$Y^2 = \frac{a}{W} \sum_{i=1}^{9} \beta_i \left(\frac{a}{W}\right)^{i-1}, \tag{A8}$$

where $\beta_i$ is a series of coefficients. Integrating Equation A6 gives

$$C\left(\frac{a}{W}\right) = \frac{2(1-\nu^2)}{Et} \int \sum_{i=1}^{9} \beta_i \left(\frac{a}{W}\right)^i d\left(\frac{a}{W}\right) + C(O) \tag{A9}$$

$$= C(O) + \frac{2(1-\nu^2)}{Et} \sum_{i=1}^{9} \frac{\beta_i}{1+i} \left(\frac{a}{W}\right)^{i+1}, \tag{A10}$$

where $C(O)$ is the value of the compliance for $a = 0$. The coefficients $\beta_i$ are obtained by calculating the $Y^2$ expression (Equation A8). The coefficients $\lambda_i = (\beta_i/1+i)$ are listed below

$\lambda 1 =$ 438.08
$\lambda 2 =$ − 3 660.53
$\lambda 3 =$ 18 306.923
$\lambda 4 =$ − 60 694.22
$\lambda 5 =$ 140 845.395
$\lambda 6 =$ −224 389.385
$\lambda 7 =$ 234 017.808
$\lambda 8 =$ −144 391.40
$\lambda 9 =$ 40 819.32.

## References


1. W. D. KINGERY, *J. Amer. Ceram. Soc.* **1** (1955) 3.
2. D. P. H. HASSELMAN, *ibid.* **11** (1969) 600.
3. A. G. EVANS, *Proc. Brit. Ceram. Soc.* **25** (1975) 217.
4. D. P. H. HASSELMAN, R. BADALIANCE, K. R. McKINNEY and C. H. KIM, *J. Mater. Sci.* **11** (1976) 458.
5. N. KAMIYA and O. KAMIGAITO, *ibid.* **14** (1979) 573.
6. J. H. McKLEE and A. M. ADAMS, *Trans. Brit. Ceram. Soc.* **49** (1950) 386.
7. American Society for Testing Materials Designation C 38-49, ASTM Comm. C-8 (1952).
8. D. P. H. HASSELMAN, E. P. CHEN and P. A. URICH, *Ceram. Bull.* **57** (1978) 190.
9. C. L. AMMANN, J. E. DOHERTY and C. G. NESSLER, *Mater. Sci. Eng.* **22** (1976) 15.
10. Y. W. MAI and A. G. ATKINS, *J. Mater. Sci.* **10** (1973) 1904.
11. J. LAMON, PhD thesis, Ecole des Mines de Paris (1978).
12. R. G. HOAGLAND, *Scripta Met.* **9** (1975) 907.
13. ASTM Standards, Part 31 (1970).
14. A. G. EVANS and E. A. CHARLES, *J. Amer. Ceram. Soc.* **60** (1977) 22.
15. S. P. TIMOSMENKO and J. N. GOODIER, "Theory of Elasticity", 3rd edn. (McGraw-Hill Book Company, New York, 1970).
16. P. P. BENHAM and R. D. HOYLE, "Thermal Stresses" (Sir Isaac Pitman and Sons Ltd, London, 1964).
17. A. G. EVANS, M. LINZER, H. JOHNSON, D. P. H. HASSELMAN and M. E. KIPP, *J. Mater. Sci.* **10** (1975) 1608.
18. S. S. MANSON and R. W. SMITH, *J. Amer. Ceram. Soc.* **38** (1955) 18.
19. D. P. H. HASSELMAN, *ibid.* **52** (1969) 600.
20. J. P. BERRY, *J. Mech. Phys. Sol.* 8 (1960) 194.
21. Plane Strain Crack Toughness Testing of High-Strength Metallic Materials, ASTM STP 410 (American Society for Testing and Materials, Philadelphia, 1967).


Received 2 December 1980 and accepted 13 January 1981.